PAPER

Human Activity Identification by Height and Doppler RCS Information Detected by MIMO Radar

Dai SASAKAWA[†], ***Student Member***, **Naoki HONMA**[†], ***Member***, **Takeshi NAKAYAMA**[††], ***and*** **Shoichi IIZUKA**[††], ***Nonmembers***

SUMMARY This paper introduces a method that identifies human activity from the height and Doppler Radar Cross Section (RCS) information detected by Multiple-Input Multiple-Output (MIMO) radar. This method estimates the three-dimensional target location by applying the MUltiple SIgnal Classification (MUSIC) method to the observed MIMO channel; the Doppler RCS is calculated from the signal reflected from the target. A gesture recognition algorithm is applied to the trajectory of the temporal transition of the estimated human height and the Doppler RCS. In experiments, the proposed method achieves over 90% recognition rate (average).

key words: *MIMO array, human activity identification, human localization, MUSIC method, microwave sensors, Doppler RCS.*

1. Introduction

Wi-Fi is now a very popular access system technology. While developed for communication Wi-Fi can also be used to realize sensing-based services. The aging society raises new social concerns such as lonely death, and the increase in the number of elderly people demands to sense systems that can observe the elderly by detecting activities such as falls. Internet of thing devices such as networked video cameras [1] or wearable sensors [2][3] can be used to monitor the elderly. However, the former violates privacy in spaces such as the bathroom and restroom, and it provides only line-of-sight coverage. The latter requires wearing sensors continuously, and so places excessive physical and mental burdens on the user. This approach is also unsuitable for the elderly because observation depends on the person remembering to wear the device.

Microwave sensing provides another approach to protecting the elderly. Its key features are privacy assurance and contact-less observation, no wearable device is needed [4]-[6]. Microwave-based monitoring can be realized by Direction of Arrival (DOA)/Direction of Departure (DOD) based Multiple-Input Multiple-Output (MIMO) radar systems [7][8]. Although such systems can localize targets, their precision is inadequate because the desired signal is interfered by undesired waves due to the multi-path environment of most private homes. We need a system/algorithm suitable for human localization in multi-path environments. Known approaches include Time Difference of Arrival (TDOA) estimation [9][10], and trigonometry methods based on DOA/DOD estimation using the MUSIC method [11]-[14]. Though TDOA localizes targets even in multi-path environments, it needs a wide-band signal of over 1.79 GHz (from 5.46 GHz to 7.25 GHz) and can only estimate the target location. Moreover, static channels are essential, i.e. the environment without humans must be measured in advance, and the measurements must be repeated if the environment is changed, e.g., a piece of furniture is shifted. The localization method based on MUSIC [11] uses a low-frequency band, 250 MHz, and estimates target location by using spherical mode MUSIC to process the oscillating return signal. Unfortunately, in this method the array aperture must be comparable to the estimated distance because of the low frequency, observation periods of over 10 seconds are necessary. DOD/DOA-based MIMO radars using the trigonometry technique [12]-[14] can localize the target by Fourier transforming the MIMO channel [15]. However, this method needs to observe the channel for several tens of seconds to accurately capture human biological information, and the only target location is estimated.

Fortunately, human activity recognition is possible by using microwave sensors [16]- [18]. These methods can estimate human activity in actual environments. [16] and [17] measure channel state information (CSI) affected by a human activity, and they identify the activity by using the characteristics of the Doppler shift of the CSI. However, these methods cannot estimate a target location, and fail to identify an activity if multiple people occupy the same environment because the Doppler effect of the activity, which is generated by multiple targets, is mixed. [18] estimates the position of the object in the house and can be used for activity recognition. However, this method cannot actually detect actions, because the position is used to identify the activity. For example, cooking is the activity associated with the position of the kitchen.

The authors have already proposed a human posture identification method that uses a MIMO array [19]. This method estimates target location in three dimensions by using the time-differential channel technique

[†]Graduate School of Engineering, Iwate University, Morioka, 020-8551, Japan.

[††]Home Appliances Development Center, Panasonic Corporation, Kadoma, 571-8504, Japan.

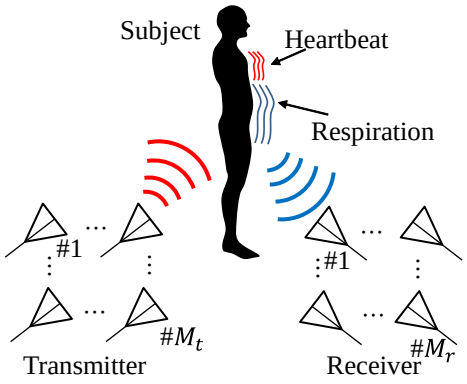

Fig. 1: Concept of microwave system for human activity identification.

[20][21]; the Doppler RCS is calculated from the power reflected from the target and the distance between the estimated location and the receiver/transmitter. Though the method can accurately estimate human location with the root mean square error (RMSE) of just 0.25 m, it handles only static targets. The authors have also studied estimating human activity from height and Doppler Radar Cross Section (RCS) information detected by MIMO radar [22][23] that uses a single frequency, 2.47 GHz. However, work reported was a just initial study, and no formal identification algorithm was described. To rectify this omission, this paper presents a complete human activity identification method that uses MIMO radar. The trajectories of the temporal transition of the estimated height and the Doppler RCS are extracted, and a gesture recognition algorithm [24] is applied to the trajectory. Experiments carried out in an actual indoor environment demonstrate that the proposed method can identify human activity with an accuracy of over 80%.

2. Human Activity Identification Using MIMO Radar

The authors previously proposed a fast localization algorithm that estimates subject location by using the time-variant channel in multi-path environments [20]. In this study, we apply the localization algorithm to the observed channel, and the three-dimensional location of the subject is estimated by MIMO radar. The Doppler RCS is calculated from the received power spectrum and the distance between the transmitter/receiver, which is calculated from the estimated target location. This algorithm detects the period of the activity from the peaks in Doppler RCS because the Doppler RCS greatly fluctuates with subject motion. After detecting the period of the activity, the gesture recognition algorithm [24] is introduced to identify the activity. The following section explains the method in detail.

2.1 Three-dimensional Human Localization

Figure 1 show the concept of our microwave system for human activity identification. This study assumes a MIMO radar with an M_r element array receiver and an M_t element array transmitter. In a multi-path environment containing one person, the time-variant channel is generated by the fluctuations of the human body's surfaces due to motion, respiration, and heartbeat. Here, the $M_r \times M_t$ time-variant MIMO channel is expressed as,

$$\boldsymbol{H}(t) = \begin{pmatrix} h_{11}(t) & \dots & h_{1M_t}(t) \\ \vdots & \ddots & \vdots \\ h_{M_r1}(t) & \dots & h_{M_rM_t}(t) \end{pmatrix}, \quad (1)$$

where, h_{ij} is the complex channel response from the j-th transmitter element to the i-th receiver element, and t represents the observation time. $M_r \times M_t$ MIMO radar can be considered to be $M_rM_t \times 1$ virtual Single-Input Multiple-Output (SIMO) radar [8]. The converted SIMO channel is expressed as,

$$\boldsymbol{h}(t) = [h_{11}(t), \dots, h_{M_r1}(t), \dots, h_{M_rM_t}(t)]^T, \quad (2)$$

where, $\{\cdot\}^T$ means transposition. DOA and DOD of the target can be estimated using this virtual SIMO channel, but unwanted path components disturb the estimates of the human location. The unwanted path components consist of the direct wave from transmitter to receiver and waves reflected from the wall, floor and furniture; fortunately, these components are static. On the other hand, the wave reflected from the human body fluctuates because of the user?s motion, respiration, and heartbeat. Therefore, the undesired components are excluded by applying the fast localization algorithm to the converted SIMO channel. This algorithm uses the time-differential channel, which is defined as,

$$\boldsymbol{h}_{sb}(t, t_{sb}) = \boldsymbol{h}(t) - \boldsymbol{h}(t + t_{sb}), \quad (3)$$

where, t_{sb} represents the time difference. Here, we calculate the averaged correlation matrix $\boldsymbol{R}$ as,

$$\boldsymbol{R} = \overline{\boldsymbol{R}_i(t, t_{sb})}, \quad (4)$$

$$\boldsymbol{R}_i(t, t_{sb}) = \boldsymbol{h}_{sb}(t, t_{sb})\boldsymbol{h}_{sb}(t, t_{sb})^H, \quad (5)$$

where, $\overline{\{\cdot\}}$ is the averaging operator, $\boldsymbol{R}_i$ represents the instantaneous correlation matrix, $\{\cdot\}^H$ means complex conjugate transposition. In (4), t and t_{sb} are averaging parameters. By eigenvalue decomposition, the averaged correlation matrix $\boldsymbol{R}$ is given by,

$$\boldsymbol{R} = \boldsymbol{U}\boldsymbol{\Lambda}\boldsymbol{U}^H, \quad (6)$$

$$\boldsymbol{U} = [\boldsymbol{u}_1, ..., \boldsymbol{u}_{M_rM_t}], \quad (7)$$

$$\boldsymbol{\Lambda} = \mathrm{diag}([\lambda_1, ..., \lambda_{M_rM_t}]), \quad (8)$$

where, $\boldsymbol{U}$ and $\boldsymbol{\Lambda}$ represent the eigenvector and the diagonal matrix representing eigenvalues, respectively. Note that the eigenvalues, Λ, are related as follows,

$$\lambda_1 > \lambda_2 = \cdots = \lambda_{M_r M_t} = \sigma_f^2 \tag{9}$$

where, σ_f^2 represents the expected value of the power of the channel component fluctuation created by noise. The eigenvector corresponding to noise, $[\boldsymbol{u}_2, \cdots, \boldsymbol{u}_{M_r M_t}]$, is expressed as $\boldsymbol{U}_N$ because one target is assumed. In this study, subject location is estimated by three-dimensional MUSIC with spherical mode vector; an extension of the original MUSIC method [7] to cover the 3D domain. The three-dimensional spherical mode vector $\boldsymbol{a}(x, y, z)$ is expressed as,

$$\boldsymbol{a}(x, y, z) = \boldsymbol{a}_t \otimes \boldsymbol{a}_r, \tag{10}$$

$$\boldsymbol{a}_t(x, y, z) = [e^{-j2\pi/\lambda D_{t1}}, \ldots, e^{-j2\pi/\lambda D_{t M_t}}]^T, \tag{11}$$

$$\boldsymbol{a}_r(x, y, z) = [e^{-j2\pi/\lambda D_{r1}}, \ldots, e^{-j2\pi/\lambda D_{r M_r}}]^T, \tag{12}$$

where, $\boldsymbol{a}_t(x, y, z)$ and $\boldsymbol{a}_r(x, y, z)$ are the steering vectors at the transmitting and receiving side, respectively. $\otimes$ represents the Kronecker product, λ is wavelength, D_{tj}/D_{ri} means the distance between position (x, y, z) and the j-th transmitter element/i-th receiver element, respectively. The evaluation function of the MUSIC method (MUSIC spectrum) is written as,

$$P(x, y, z) = \frac{\boldsymbol{a}^H(x, y, z)\boldsymbol{a}(x, y, z)}{\boldsymbol{a}^H(x, y, z)\boldsymbol{U}_N\boldsymbol{U}_N^H\boldsymbol{a}(x, y, z)}. \tag{13}$$

The MUSIC spectrum peak represents the estimated target location.

2.2 Calculating Doppler RCS

The first eigenvector, $\boldsymbol{u}_1$, of (7) corresponds to target location. The converted SIMO channel, $\boldsymbol{h}(t)$, (2) and the first eigenvector, $\boldsymbol{u}_1$, are multiplied to enhance the biological component of the target, and this signal, $y(t)$, is expressed as,

$$y(t) = \boldsymbol{u}_1^H \boldsymbol{h}(t) s, \tag{14}$$

where s is the transmitted signal, which is a continuous wave, i.e. s is a constant value in this study. The observed signal, $y(t)$, is Fourier-transformed, and is defined as $F(\omega)$. Then, the received power, $P_r(\omega)$ is expressed as,

$$P_r(\omega) = \frac{|F(\omega)|^2}{M_r M_t}, \tag{15}$$

where, ω represents frequency. Here, the Doppler radar cross section (RCS) is defined by solving the radar range equation for σ; this is expressed as,

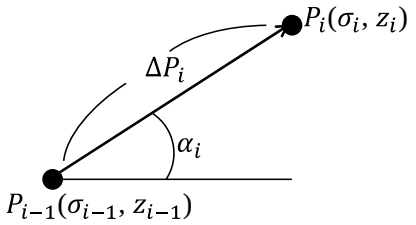

Fig. 2: Moving distance, ΔP_i, and the direction of movement, α_i.

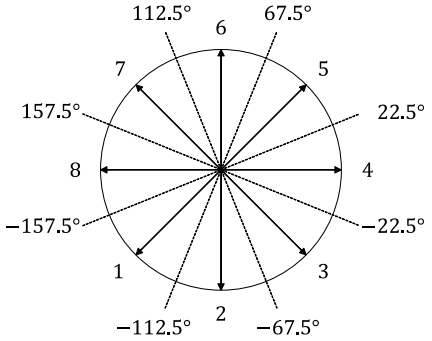

Fig. 3: Determination of the direction code when the division number of direction code, N_d, is 8.

$$\sigma = \frac{(4\pi)^3 r_r^2 r_t^2}{G_r G_t \lambda^2 P_t} \int_{f_1}^{f_2} P_r(\omega) d\omega, \tag{16}$$

$$r_r = \sqrt{(x_e - X_r)^2 + (y_e - Y_r)^2 + (z_e - Z_r)^2}, \tag{17}$$

$$r_t = \sqrt{(x_e - X_t)^2 + (y_e - Y_t)^2 + (z_e - Z_t)^2}), \tag{18}$$

where, r_r and r_t represent the distances of the estimated target location from the centers of the receiver and transmitter antennas, respectively. (x_e, y_e, z_e) is the estimated location of the target. (X_r, Y_r, Z_r) and (X_t, Y_t, Z_t) are the center of the receiver and transmitter antennas, respectively. P_t represents the transmitting power and G_r and G_t are the gain of receiving antenna and transmitting antenna, respectively. f_1 and f_2 define the frequency range that encompasses the vital sign effects.

2.3 Human Activity Identification Using Gesture Recognition Algorithm

We obtain the estimated location and the Doppler RCS by (13) and (16), respectively. The Doppler RCS greatly fluctuates during the subject action. Therefore, this algorithm detects the period of the activity by searching the large Doppler RCS. After detecting the period of the activity, the gesture recognition algorithm [24] is used to identify the human activity. Then,

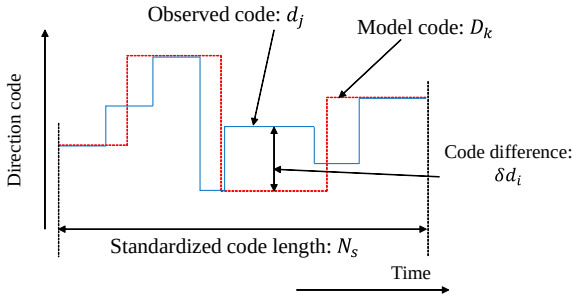

Fig. 4: Concept of comparing model code D_k to observed code d_j.

the temporal transition of height, z_i, and Doppler RCS, σ_i, is obtained by continuous estimation, where z_i and σ_i represent the i-th estimated height and i-th calculated Doppler RCS, respectively. Figure 2 shows the moving distance, ΔP_i, and the direction of movement, α_i; they are defined as,

$$\Delta P_i = \sqrt{(\sigma_i - \sigma_{i-1})^2 + (z_i - z_{i-1})^2}, \tag{19}$$

$$\alpha_i = \tan^{-1} \frac{z_i - z_{i-1}}{\sigma_i - \sigma_{i-1}}. \tag{20}$$

The trajectories of the height and Doppler RCS are given by (19) and (20).

Direction codes are determined from the direction of movement, α_i, between the two sampled points on the trajectory. Figure 2 shows that the direction code corresponds to the movement, α_i; the division number of direction code, N_d, is 8 in this study. Figure 3 shows the determination of the direction code in this study. However, the number of trajectory points differs even for the same activity because the speeds of the activity are not same for all trials. For this reason, the length of the direction code is normalized regardless of the trajectory speed. A normalized code, D_k, is generated from original direction code d_j by considering the code length and the period of the activities, where the lengths of normalized code D_k and original direction code d_j are N_s and N_o, respectively. Here, code lengths N_s and N_o satisfies the relation,

$$N_o \leq N_s. \tag{21}$$

The flow of conversion from the original code d_j to the standardized code D_k is shown below.
i) When the index j (j: index number in the raw code) is 1, the normalized code D_k is defined as,

$$D_k = d_1$$

$$(1 \leq k \leq \frac{\Delta P_1}{\Delta P_{sum}} \times N_s), \tag{22}$$

$$\Delta P_{sum} = \sum_{j=1}^{N_o} \Delta P_i, \tag{23}$$

where, k is the index number in the normalized code.
ii) When the index range is $2 \leq j \leq N_o$, the normalized code D_k is defined as,

$$D_k = d_j,$$

$$(\frac{\sum_{i=1}^{j-1} \Delta P_i}{\Delta P_{sum}} \times N_s < k \leq \frac{\sum_{i=1}^{j} \Delta P_i}{\Delta P_{sum}} \times N_s). \tag{24}$$

Then, the trajectory is converted into the direction code. The training data of all actions is made and identified. An observed trajectory is converted into the appropriate direction code, and the deviation from all training codes is calculated. The model codes were generated from the most frequent values of the feature as discovered in 10 trials for each motion, and the generated model code is defined as D_{model}.

Figure 4 shows the concept of comparing the model code and an observed code, where the normalized code of the observed activity is defined as d_{test}. The sum of squared deviation, E, which is used for activity identification, is defined as,

$$E = \sum_{l=1}^{N_s} \delta d_l^2, \tag{25}$$

$$\delta d_l = |d_{test,l} - D_{model,l}|, \tag{26}$$

where, $d_{test,l}$ and $D_{model,l}$ represent the l-th direction codes of the observation code and the model code, respectively. However, since the direction code is circular as shown in Fig. 2, the maximum difference in the direction code that can be taken is one half of the direction division number N_d, i.e. 4 in this study. Therefore, when $\delta d_l \geq N_d/2$, δd_l is replaced as follows,

$$d_l = N_d - \delta d_l. \tag{27}$$

The sum of squared deviation, E, is calculated for the model code of each activity, and the current action is classified to one of the learned actions by finding the training code with minimum deviation from the current one.

The agility and accuracy of the estimation have a trade-off relationship. In this study, the observation time should be short to detect human activity, but then

Table 1: Measurement conditions.

Antenna element (Tx/ Rx)	16-element patch antenna
Distance between Tx and Rx, d	4 m
Height of the Tx/ Rx, h	1.0 m
Frequency	2.47125 GHz
Tx power	-10 dBm
Snapshot rate	100 Hz
Channel measurement period	0.64 s
Interval of localization and calculating Doppler RCS	0.25 s

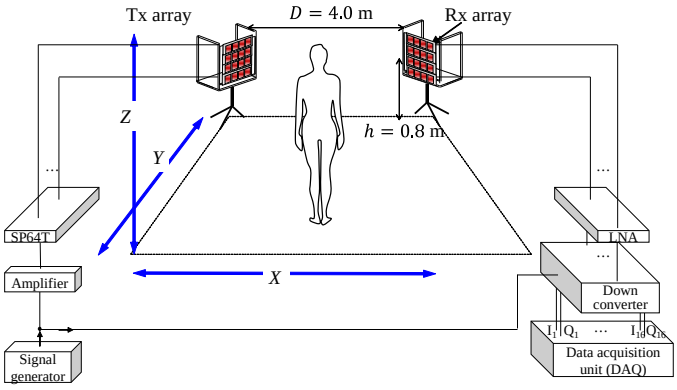

Fig. 5: Measurement overview.

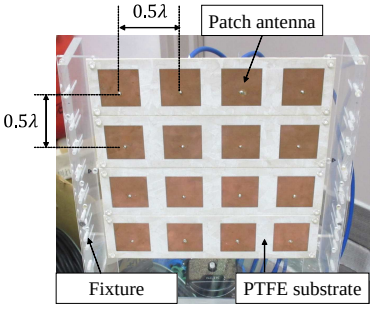

Fig. 6: Photo of MIMO array.

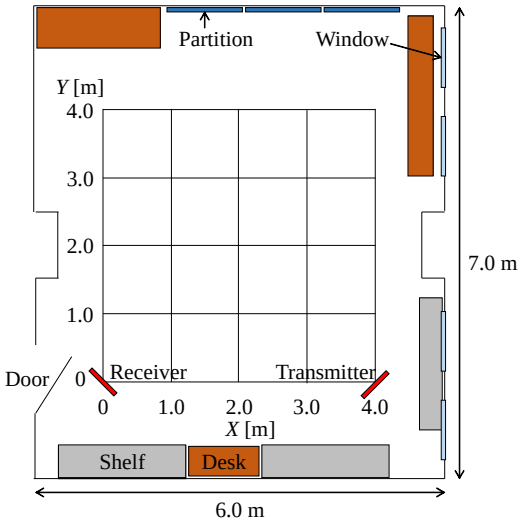

Fig. 7: Experimental room with concrete walls; its width, depth and height were 7.0, 6.0 and 2.7 m, respectively.

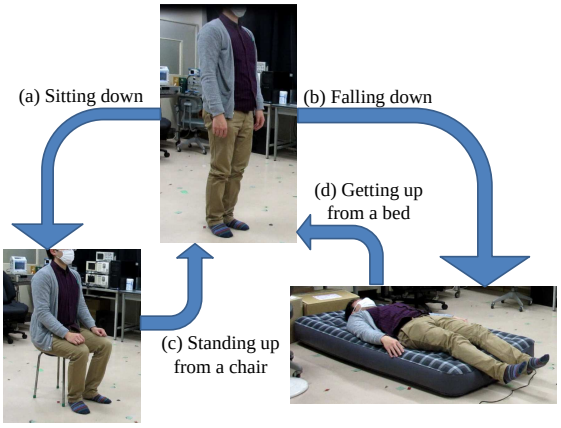

Fig. 8: Human activities tested.

the estimated values vary widely. Therefore, a filtering technique is applied to the estimated values to improve identification accuracy.

3. Experimental Condition and Measurement Setup

Table 1 and Figure 5 overview the measurement setup. The element space of the arrays of receiver and transmitter was one half the wavelength. The distance between transmitting and receiving antennas was set to 4.0 m. The receiver and the transmitter were directed to the center of the room. As shown in Figure 5, a Single-Pole 64 Throw (SP64T) switch was used at the transmitting side. Though the exact observation moment is not the same for all elements in the MIMO channel matrix, the time differences among the elements are so short compared to the vital and moving activity that they can be ignored. A continuous wave (CW) signal of 2.47125 GHz was used; the transmitting power was set to -10 dBm. The CW signal was split to the down-converter at the receiver side since accurate synchronization between transmitting and receiving sides is needed. At the receiver side, received signals are input to a down-converter unit by way of a Low-Noise Amplifier (LNA) unit. The down-converted baseband signals (I_1, Q_1,~I_{16}, Q_{16}) were digitized by a data-acquisition unit (DAQ) with sampling frequency of 20 kHz. The snapshot rate of the MIMO channel is determined by the switching speed of the SP64T. In the experiments, the rate for taking a snapshot of the MIMO channel was set to 100 Hz. In this study, the observation period for localization and calculating Doppler RCS was set to 0.64 seconds. Thus the number of snapshots per single observation period was 64. The

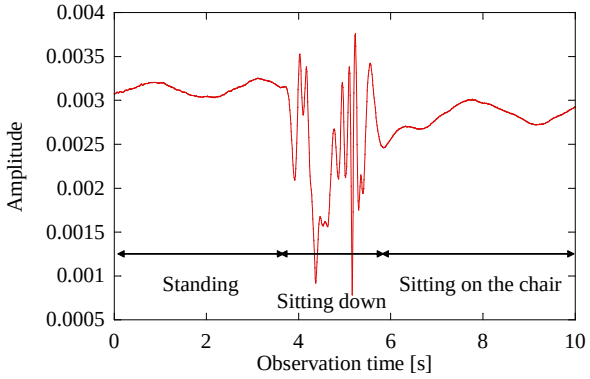

Fig. 9: Example of the time-variant channel response for target activity of sitting down.

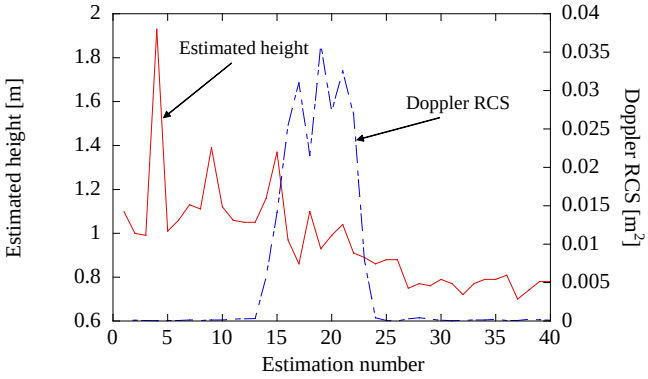

Fig. 10: Temporal transition in estimated height and the Doppler RCS.

transmission components of S parameters were used as the propagation channel. Figure 6 shows a photo of the array antenna used as the receiver and the transmitter. 16×16 MIMO radar was used in the experiment. The receiver and transmitter have 4×4 patch antennas on a square grid. All array antennas used a PTFE substrate, and antenna thickness, width, and height were 1.6, 60 and 240 mm, respectively. These elements have a vertical polarization. The array's center was set to $h = 1.0$ m, which corresponds to the torso height of the subjects. The number of targets was determined following the MUSIC method. The normalized code length N_s was set to 100. In this study, time difference t_{sb} was set to 0.05 [s] $\leq t_{\mathrm{sb}} \leq$ 0.63 [s] for localization, while the range of frequency was set from 1.56 Hz to 10.94 Hz in calculating the Doppler RCS; antenna gain G_r and G_t was 4.96 dB, which is the average gain value from $-40°$ to $40°$. Figure 7 shows the experimental room. The experiment was carried out in a room containing desks and shelves. The room had concrete walls and its width, depth and height were 7.0, 6.0 and 2.7 m, respectively. The measurement location of the target was set to $(x, y) = (2.0, 2.0)$ [m].

Figure 8 shows the human activities tested in this campaign. While the channels were being captured, the subject performed 4 activities: sitting down (a), falling down (b), standing up from a chair (c), and getting up from a bed(d). The model codes were generated from the most frequent values of the feature observed in 10 trials for each motion, and the recognition rate with all motions was calculated using 10 recognition experiments (all activities).

4. Experimental Results

Figure 9 shows an example of the time-variant channel response, h_{11}, of the observed channel when the target sat down. In this figure, the channel variation exhibits the periodic biological activities such as respiration before and after action. Obviously, the channel widely

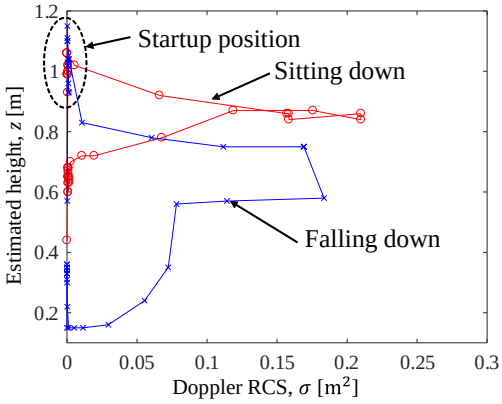

Fig. 11: Example of the trajectory of the estimated height and Doppler RCS for subject activities of sitting down and falling down.

Table 2: Average recognition rates of the human activity for all filters.

Filter	Recognition rate
No filter	82.5%
Median (fourth-order)	80%
Moving average(fourth-order)	92.5%

changes during sitting down.

Figure 10 shows the temporal transition in the estimated height and the Doppler RCS when the channel of Figure 9 was used. This figure shows that the human activities yielded large Doppler RCS. The estimated height values were about 1 meter in the first half, and the estimated height values were lower than previous state after sitting down. On the other hand, the estimated height exhibits significant variation because of the short observation time.

Figure 11 shows an example of the trajectory of the estimated height and Doppler RCS when the subject sat down and fell down. Note that the subject was standing still before those actions, and the figure shows that the start values of the estimated height are

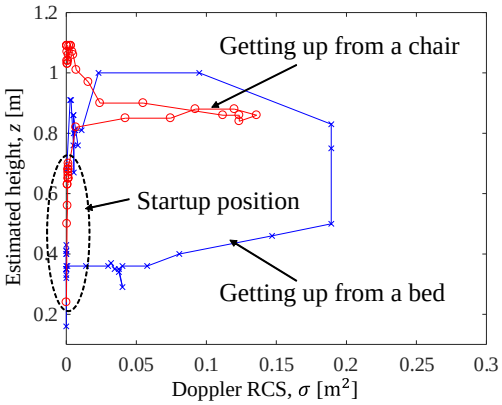

Fig. 12: Example of the trajectory of the estimated height and Doppler RCS for the activities of standing up from a chair and getting up from a bed.

clustered near 1.0 m. The two activities yielded different trajectories. With activity completion, the estimated heights of sitting down and falling down clustered around 0.7 m and 0.2 m, respectively.

Figure 12 shows an example of the trajectory of the estimated height and Doppler RCS for the subject activities of standing up from a chair and getting up from a bed. The initial positions for these activities were sitting on the chair and lying on the bed, respectively. The figure shows that the initial values of the activities of standing up from a chair and getting up from a bed clustered around 0.7 m and 0.3 m, respectively. The action of the standing up from a chair showed a sharp trajectory. On the other hand, the action of getting up from a bed yielded a trace like a circle. After the action, the both estimated heights gathered near 1.0 m.

Fig. 13 shows an example of the trajectory of the estimated height and Doppler RCS when the target sat down. Figure 13(a) show the trajectory without any filter, Figure 13(b) and (c) show the results processed by the fourth-order median filter and the fourth-order moving average filter, respectively. In this figure, the trajectories yielded by using raw values vary widely because the observation time used to estimate location and Doppler RCS is short. On the other hand, the filtered trajectories exhibit no outliers and reduced dispersion.

Figure 14 shows the training code and test data for the activity of sitting down. The training code was taken to be most frequent value recorded in 10 trials. This figure shows that the test data well agrees with the training code, and in this test the activity was correctly identified as sitting-down motion. Table 2 shows the averaged recognition rate of the human activity for all filters. The averaged recognition rate is the mean value of the identification rate of all motions. In this table, the recognition rate with no filter was 82.5%.

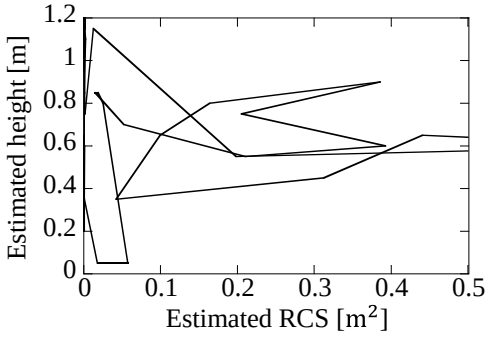

(a) No filter.

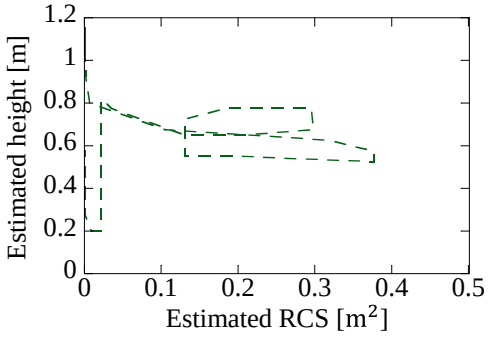

(b) Median filter.

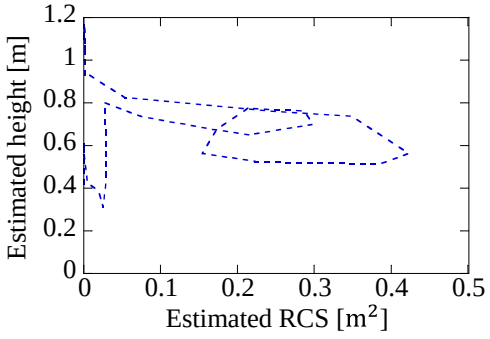

(c) Moving average filter.

Fig. 13: Example of the trajectory of the estimated height and Doppler RCS with/without filter.

In comparison, the averaged recognition rate with the fourth-order median filter was 80% (lower than the rate with no filter); while the result with the fourth-order moving average filter was 92.5%, a significant improvement in the recognition rate.

Fig.15 shows the confusion matrix of the recognition rate of the result with the moving average filter. From this figure, all recognition rates exceeded 80%. To validate the effectiveness of the proposed method, we evaluated the recognition performance of another algorithm, where the temporal correlation between the training and test data is used. In this algorithm, the observed activity is classified as the training activity with maximum correlation. Figure 16 shows the confusion

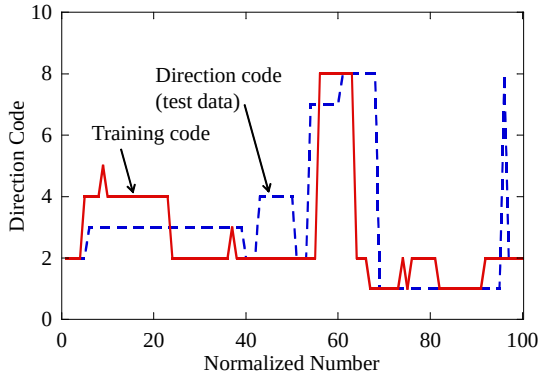

Fig. 14: Training code and test data.

		Predicted activity			
		Sitting down	Falling down	Standing up from a chair	Getting up from a floor
Actual activity	Sitting down	1	0	0	0
	Falling down	0.1	0.8	0	0.1
	Standing up from a chair	0	0	0.9	0.1
	Getting up from a floor	0	0	0	1

Fig. 15: Confusion matrix of the recognition rate of the result with moving average filter.

		Predicted activity			
		Sitting down	Falling down	Standing up from a chair	Getting up from a floor
Actual activity	Sitting down	0.4	0.6	0	0
	Falling down	0.3	0.6	0	0.1
	Standing up from a chair	0.4	0.2	0.4	0
	Getting up from a floor	0.3	0.2	0.1	0.4

Fig. 16: Confusion matrix of the recognition rate of the raw observation channel.

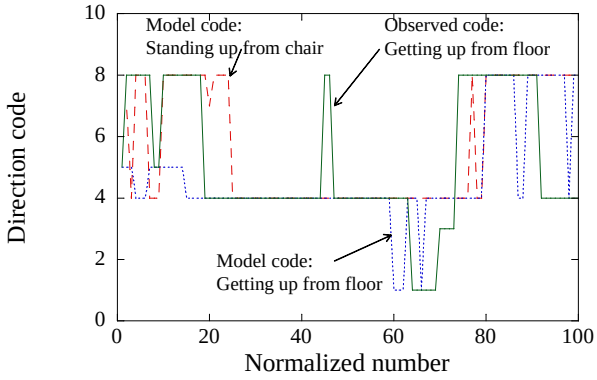

Fig. 17: Example of prediction error, when the activity was "getting up from the floor", and this was identified as "standing up from a chair".

matrix of the recognition rate of the correlation-based algorithm. From this figure, the maximum recognition rate was 60% for falling down, and the average recognition rate was 45%. This result shows that the proposed method achieves highly accurate activity identification.

Figure 17 shows an example of the prediction error. In this figure, the observed activity was getting up from the floor, while the identified activity was standing up from a chair. As can be seen from the figure, the model codes of both activities are similar, and this caused prediction error. These errors can be reduced by estimating the posture before and after the activity and to correct incorrect decisions.

5. Conclusion

This paper proposed and demonstrated a human activity identification method that is based on estimating the height and Doppler RCS information from MIMO radar data. In this paper, we introduced three-dimensional localization and calculation of the Doppler RCS. A gesture recognition algorithm was applied to the trajectory of the temporal transitions of the estimated height and the Doppler RCS. Experiments showed that the highest recognition rate was 92.5% on average for the classification of four common activities: sitting down, falling down, standing up from a chair, and getting up from a bed. This proves that the proposed method well estimates human activities in the home. This paper assumes an environment containing only one target, while a realistic environment often contains multiple targets. When there are multiple targets in the same environment, the targets' signals are mixed in the observed channel. Therefore, the human activity identification requires to distinguish the multiple targets' signals. In our future work, we will study an algorithm for detecting multiple targets' activities in a realistic environment.

References

[1] L. Fiore, D. Fehr, R. Bodor, A. Drenner, G. Somasundaram, and N. Papanikolopoulos, "Multi-camera human activity monitoring," Jour. of Intelligent and Robotic Systems, Vol.52 No.1, pp. 5-43, 2008.

[2] SW. Lee, and K. Mase, "Activity and location recognition using wearable sensors," IEEE pervasive computing Vol.1, No.3, pp. 24-32, 2002.

[3] S. Patel, H. Park, P. Bonato, L. Chan, and M. Rodgers, "A review of wearable sensors and systems with application in rehabilitation," Journal of neuroengineering and rehabilitation, Vol. 9, No. 1, 2012.

[4] J. C. Lin, "Noninvasive microwave measurement of respira-

tion," Proceedings of the IEEE, Vol. 63, No. 10, pp. 1530-1530, 1975.

[5] A. Droitcour, V. Lubecke, J. Lin, and O. Boric-Lubecke, "A microwave radio for Doppler radar sensing of vital signs," In Microwave Symposium Digest, 2001 IEEE MTT-S Int., Vol. 1, pp. 175-178, May, 2001.

[6] H. Avagyan, A. Hakhoumian, H. Hayrapetyan, N. Pogosyan, and T. Zakaryan, "Portable non-contact microwave Doppler radar for respiration and heartbeat sensing," Armenian Journal of Physics Vol.5, No.1, pp.8-14, 2012..

[7] R. Schmidt, "Multiple emitter location and signal parameter estimation," IEEE Transactions on Antennas and Propagation, Vol. 34, Issue 3, pp. 276-280, Mar. 1986.

[8] J. Li, P. Stoica, "MIMO radar signal processing," A John Wiley & Sons inc., 2009.

[9] F. Adib, Z. Kabelac, D. Katabi, and R. C. Miller, "3D Tracking via Body Radio Reflections," In NSDI, Vol. 14, pp. 317-329, Apr. 2014.

[10] F. Adib, Z. Kabelac, and D. Katabi, "Multi-person motion tracking via RF body reflections," 2014.

[11] T. Miwa, S. Ogiwara, and Y. Yamakoshi, "Localization of living-bodies using single-frequency multistatic Doppler radar system," IEICE transactions on communications, Vol.92, No.7, pp.2468-2476, 2009.

[12] D. Sasakawa, K. Konno, N. Honma, K. Nishimori, N. Takemura, T. Mitsui, and T. Tsunekawa, "Localizing living body using bistatic MIMO radar in multi-path environment," Antennas and Propag. (EuCAP), 2014 8th European Conference on. IEEE, pp. 3253-3257, Apr. 2014.

[13] K. Konno, N. Honma, D. Sasakawa, Y. Tsunekawa, K. Nishimori, N. Takemura, and T. Mitsui, "Localizing multiple target using bistatic MIMO radar in multi-path environment," In Electromagnetics (iWEM), 2014 IEEE Int. Workshop on. IEEE, pp. 90-91, Aug. 2014.

[14] K. Konno, N. Honma, D. Sasakawa, K. Nishimori, N. Takemura, T. Mitsui, and Y. Tsunekawa, "Estimating living-body location using bistatic MIMO radar in multi-path environment," IEICE Trans. on Communications, Vol. 98, No. 11, pp. 2314-2321, 2015.

[15] K. Konno, M. Nango, N. Honma, K. Nishimori, N. Takemura, and T. Mitsui, "Experimental evaluation of estimating living-body direction using array antenna for multipath environment," IEEE Antennas and Wireless Propag. Lett., Vol. 13, pp. 718-721, 2014.

[16] Q. Pu, S. Gupta, S. Gollakota, and S. Patel, "Whole-home gesture recognition using wireless signals," Proceedings of the 19th annual international conference on Mobile computing & networking. ACM, pp.27-38, Sep. 2013.

[17] W. Wang, A. X. Liu, M. Shahzad, K. Ling, and S. Lu, "Understanding and modeling of wifi signal based human activity recognition," In Proceedings of the 21st annual international conference on mobile computing and networking, ACM, pp. 65-76, Sep. 2015.

[18] Y. Wang, J. Liu, Y. Chen, M. Gruteser, J. Yang, and H. Liu, "E-eyes: device-free location-oriented activity identification using fine-grained wifi signatures," In Proceedings of the 20th annual international conference on Mobile computing and networking, ACM, pp. 617-628, Sep. 2014.

[19] D. Sasakawa, N. Honma, T. Nakayama, and S. Iizuka, "Human posture identification using a MIMO array," MDPI electronics, 7(3), 37, Mar. 2018.

[20] D. Sasakawa, K. Konno, N. Honma, K. Nishimori, N. Takemura, and T. Mitsui, "Fast estimation algorithm for living body radar," 2014 International Symposium on Antennas and Propagation (ISAP 2014), FR3D, pp. 583-584, Dec. 2014.

[21] D. Sasakawa, N. Honma, T. Nakayama, and S. Iizuka, "Fast living-body localization algorithm for MIMO radar in multi-path environment," IEEE Transactions on Antennas and Propagation, in press.

[22] D. Sasakawa, N. Honma, T. Nakayama, and S. Iizuka, "Human activity estimation by height and RCS information detected by MIMO radar," 2017 IEEE AP-S Symposium on Antennas and Propagation and USNCURSI Radio Science Meeting, Jul. 2017.

[23] D. Sasakawa, N. Honma, T. Nakayama, and S. Iizuka, "Evaluation of filtering technique for human activity identification using MIMO radar," 2017 International Symposium on Antennas and Propagation (ISAP2017), POS 3, pp. 1324-1325, Nov. 2017.

[24] T. Asano, A. Miyata, and S. Honda, "Visual interface system using character handwriting gestures," J. JSPE, Vol. 77, No. 3, pp. 333-337, Sep. 2011.